

This discussion paper is/has been under review for the journal Geoscientific Instrumentation, Methods and Data Systems (GI). Please refer to the corresponding final paper in GI if available.

A sensitivity study for far infrared balloon-borne limb emission sounding of stratospheric trace gases

J. Xu, F. Schreier, P. Vogt, A. Doicu, and T. Trautmann

DLR – German Aerospace Center, Remote Sensing Technology Institute, Oberpfaffenhofen, 82234 Weßling, Germany

Received: 29 January 2013 – Accepted: 1 May 2013 – Published: 14 May 2013

Correspondence to: J. Xu (jian.xu@dlr.de)

Published by Copernicus Publications on behalf of the European Geosciences Union.

251

Abstract

This paper presents a sensitivity study performed for trace gases retrieval from synthetic observations by TELIS (TERahertz and submillimeter Lmb Sounder) which is a stratospheric balloon-borne cryogenic heterodyne spectrometer. Issues pertaining to hydroxyl radical (OH) retrieval from the far infrared measurements by the 1.8 THz channel are addressed. The study is conducted by a retrieval code PILS (Profile Inversion for Limb Sounding) developed to solve the nonlinear inverse problems arising in the analysis of infrared/microwave limb sounding measurements. PILS combines a line-by-line forward model with automatic differentiation for computing Jacobians and employs regularized nonlinear least squares inversion. We examine the application of direct and iterative regularization methods and evaluate the performance of single- and multi-profile retrievals. Sensitivities to expected errors in calibration procedure, instrumental knowledge and atmospheric profiles have been analyzed. Nonlinearity effect, inaccurate sideband ratio, and pointing error turned out to be the dominant error sources. Furthermore, the capability of multi-channel simultaneous retrieval from the far infrared and submillimeter data has been investigated. The errors and averaging kernels infer that the quality of the obtained hydrogen chloride (HCl) can be improved by significantly better exploitation of information from the observations.

1 Introduction

Far infrared and submillimeter limb sounding is a well-established technique for atmospheric remote sensing because numerous trace gases have features in this spectral range. Furthermore, emission observations are independent of sunlight and hence can contribute to the understanding of the diurnal cycles of chemical processes. In addition, aerosols and ice clouds have negligible effect, which also makes the far infrared and submillimeter observations advantageous. The latest spaceborne missions comprise SMR (Sub-Millimetre Radiometer) (Murtagh et al., 2002) on the Odin

252

satellite launched in 2001, MLS (Microwave Limb Sounder) (Waters et al., 2006) in 1991 and 2004 aboard the UARS and Aura satellites, respectively, and SMILES (Superconducting submillimeter-wave Limb-Emission Sounder) (Kikuchi et al., 2010) from October 2009 to April 2010. In particular, Aura/MLS has the ability to measure thermal emission from the far infrared (Terahertz) spectral range.

TELIS (TErahertz and submillimeter Limb Sounder) is a new balloon-borne cryogenic heterodyne spectrometer designed to investigate the vertical distribution of stratospheric trace gas species associated with ozone depletion and climate change. The instrument utilizes state-of-the-art superconducting heterodyne technology and allows limb sounding of the Earth's atmosphere with high spectral resolution and long flight duration. TELIS was mounted on a stratospheric balloon gondola together with the MIPAS-B (Michelson Interferometer for Passive Atmospheric Sounding - Balloon) instrument (Friedl-Vallon et al., 2004), developed by the Karlsruhe Institute of Technology (KIT), and mini-DOAS (Differential Optical Absorption Spectrometer) operated by the University of Heidelberg. From a flight altitude of 30–40 km, TELIS scans the stratosphere and upper troposphere with 1.5–2 km altitude sampling. The combination of TELIS and MIPAS-B yields a wide range of the electromagnetic spectrum for atmospheric research and offers great synergies for cross-validation of measured chemical constituents. In addition, TELIS serves as a technology demonstrator to future spaceborne limb sounders. The instrument has participated in three scientific campaigns in Kiruna, Sweden from March 2009 to March 2011.

TELIS was developed by a consortium of European institutes that include the German Aerospace Center (DLR), the Netherlands Institute for Space Research (SRON), and the Rutherford Appleton Laboratory (RAL) in the United Kingdom. The ambitious spectral coverage of the TELIS instrument is accomplished by use of three frequency channels: a highly compact 500 GHz channel, a 480–650 GHz channel (de Lange et al., 2010) based on the Superconducting Integrated Receiver (SIR) technology, and a tunable 1.8 THz channel (Suttiwong et al., 2009) with enhanced stability provided by RAL, SRON, and DLR, respectively. The incoming atmospheric radiation is transmitted from

253

a dual offset Cassegrain telescope through the front-end transfer optics where the signals are separated and coupled into each dedicated channel (Suttiwong, 2010).

The 1.8 THz channel measures the signal at a local oscillator (LO) frequency f_{LO} between 1790 and 1880 GHz. The measured spectrum is then generated from the two sidebands with respect to the LO frequency since the TELIS instrument operates in double sideband (DSB) mode. In case of the 1.8 THz channel the spectrum is recorded in the intermediate frequency f_{IF} domain ranging from approximately 4 to 6 GHz (2 GHz spectral bandwidth). The signal is split into four 500 MHz autocorrelator segments. Thus, the measured spectrum covers the frequency domains at $f_{LO} - f_{IF}$ and $f_{LO} + f_{IF}$. For the 480–650 GHz channel f_{IF} ranges from 5 to 7 GHz.

The primary scientific goal of the TELIS/MIPAS-B/mini-DOAS flight has been to measure the time-dependent chemistry of chlorine (Cl) and bromine (Br), and to achieve the closure of chemical families (NO_y , Cl_y , Br_y , HO_x) inside the polar vortex. Regarding the TELIS instrument, the main target of the 1.8 THz channel is the hydroxyl radical (OH). Further stratospheric species HO_2 , HCl, HOCl, O_3 , O_2 , CO, NO, NO_2 , and H_2O including its isotopologues can also be measured in the frequency range of 1790–1880 GHz. OH is a key reactive species for photochemical reactions that regulate ozone throughout most of the stratosphere and mesosphere. The demand and interest of having the capability to measure the OH radical in the atmosphere has been consequently increasing.

OH possesses pairs of triplets in the far infrared spectral region, such as 61 cm^{-1} (1.8 THz), 83 cm^{-1} (2.5 THz), 101 cm^{-1} (3.0 THz), 118 cm^{-1} (3.5 THz). Carli et al. (1989) and Carlotti et al. (2001) observed the 3.5 THz feature with a balloon-borne far infrared Fourier Transform spectrometer. Pickett and Peterson (1993) used a balloon-borne two-channel (101 and 118 cm^{-1}) Fabry-Perot instrument "FILOS" to retrieve stratospheric OH, and middle to upper stratospheric OH concentrations were estimated from thermal emission far infrared (83 – 230 cm^{-1}) observations with the balloon-borne "FIRS" Fourier transform spectrometer (Jucks et al., 1998). In August 1997, the air-borne heterodyne spectrometer THOMAS performed OH observations between about

254

30 and 90 km over a full diurnal cycle (Englert et al., 2000). The characterization of OH diurnal variability in the stratosphere and mesosphere has also been analyzed using measurements from the Aura/MLS instrument (Minschwaner et al., 2011). Both instruments observe OH at 2.5 THz, whereas TELIS selected 1.8 THz for monitoring OH in the lower and middle stratosphere. Although the OH emission at 1.8 THz is weaker than that at 2.5 THz, the former one was chosen for the sake of higher sensitivity of the HEB (Hot Electron Bolometer) mixer at 1.8 THz and risks associated with the development of the 2.5 THz solid state local oscillator (Mair et al., 2004).

For being able to analyze the TELIS (or further spaceborne, e.g. SMILES, Odin/SMR) measurements and retrieve trace gas profiles, the Remote Sensing Technology Institute at DLR has developed a retrieval code PILS (Profile Inversion for Limb Sounding) dedicated to high resolution infrared/microwave radiative transfer calculation and reliable inversion scheme. In this paper, we present the physical and mathematical basics of PILS as well as its capability of trace gas retrievals from synthetic TELIS measurements. Particular emphasis is placed on the capability study of the 1.8 THz channel. For a study of the 480–650 GHz channel we refer to de Lange et al. (2009). The forward model used to simulate the measurements and the inversion methodology with diagnostics are described in Sect. 2. In Sect. 3 we firstly discuss the performance of OH vertical profile retrieval from a single limb scan with perfect instrumental knowledge. A sensitivity analysis is then conducted to estimate the impact of uncertainties in calibration procedure, the atmospheric and instrument parameters in the forward model. Section 4 identifies the capability of multi-channel simultaneous processing by implementing HCl retrieval. A summary and an outlook to future work and products are given in Sect. 5.

2 Forward model and inversion methodology

2.1 Radiative transfer and instrument modelling

In atmospheric remote sensing, the radiation seen by a sensor is described by the theory of radiative transfer with an appropriate instrument model, accounting for spectral response, field-of-view, and – in case of heterodyne – the sideband ratio. Neglecting scattering and assuming local thermodynamical equilibrium, the intensity (radiance) I at wavenumber ν at position s along the line-of-sight is given by the integral form of the Schwarzschild equation (Liou, 2002; Zdunkowski et al., 2007)

$$I(\nu, s) = I(\nu, s_0) e^{-\tau(\nu; s_0, s)} + \int_{s_0}^s ds' B(\nu, T(s')) e^{-\tau(\nu; s', s)} \alpha(\nu, s'), \quad (1)$$

where $I(\nu, s_0)$ is the source radiation at position s_0 , and $B(\nu, T)$ represents the Planck function at temperature T . The optical depth τ is defined as the path integral of the volume absorption coefficient $\alpha(\nu, s)$ which is essentially the product of molecular cross section k and number density summed over the molecule. For high resolution a line-by-line evaluation is considered, i.e. k is computed by summing over the contributions from many lines: $k(\nu; \rho, T) = \sum_l S_l(T) g(\nu; \hat{\nu}_l, \gamma_l(\rho, T))$, where each line is characterized by its position $\hat{\nu}_l$, the temperature-dependent line strength $S(T)$, and a Voigt line shape function g (with half width γ) describing the combined effect of pressure (ρ) broadening and Doppler broadening.

The subsequent step is to model the instrument performance as precisely as possible. For the 1.8 THz channel, the monochromatic spectrum is convolved with an instrumental line shape function yielded by Fourier transform of a Hamming apodization function. For the 480–650 GHz channel, a Lorentzian line shape function defined by the frequency locking (de Lange et al., 2009) is used. Moreover, a superposition of pencil-beam spectra can be done by convolving with an angle-dependent field-of-view function which is Gaussian shaped with a vertical full width half maximum (FWHM) of

3.2.1 One-profile retrieval

First of all, we consider only OH as target molecule (with accurate a priori knowledge of O_3 and H_2O) to clarify the retrieval capability of the selected microwindow. The estimation of an appropriate regularization parameter plays an important role in finding a reliable retrieval solution. For this purpose, we solve the one-profile retrieval problem for various regularization parameters λ , and for each λ the relative solution errors $\epsilon(\lambda) = \|\mathbf{x}_\lambda - \mathbf{x}_t\|/\|\mathbf{x}_t\|$ are computed. In Fig. 4a we illustrate the relative solution errors of OH volume mixing ratio (VMR) for Tikhonov regularization, the iteratively regularized Gauss–Newton method, and the regularizing Levenberg–Marquardt method. For iterative methods, λ is the initial value of the regularization parameter, while at all subsequent iteration steps, the regularization parameters are the terms of a geometric sequence with the ratio $q = 0.8$. The error curve corresponding to Tikhonov regularization possesses a minimum, and by convention, the minimizers of the solution errors represent the optimal values of the regularization parameter.

Still the iteratively regularized Gauss–Newton method yields reliable results for large initial values of the regularization parameter. Evidently, a stronger regularization at the beginning of the iterative process requires a larger number of iterations as can be seen in Fig. 4b. The regularizing Levenberg–Marquardt method is also insensitive to overestimations of the regularization parameter. However, the results in Fig. 4 illustrate that the regularizing Levenberg–Marquardt method is inferior to the iteratively regularized Gauss–Newton method: for large initial values of the regularization parameter, the solution errors are larger. Henceforth, we choose Tikhonov regularization essentially for efficiency reasons as it converges quickly (with ≤ 5 iteration steps) disregarding any choice of λ .

For $\lambda = 1 \times 10^{-4}$, the retrieved OH concentration profile along with the corresponding quantity in terms of relative difference is plotted in Fig. 5a. The relative difference is up to 12% (at 15 km) in the plotted altitude range. The quality of the retrieval is also assessed by the retrieval error encapsulating the combined effect of the noise and the

265

smoothing errors (Fig. 5b). The smoothing error dominates the retrieval error budget from 15 to 27.5 km where the noise error is fairly small, which implies that the retrieval error at these altitudes relies on the a priori information and the vertical resolution is poor. The noise error as the main error stretches from 27.5 km upward, while the smoothing error appears to take less effect.

3.2.2 Two-profile retrieval

For the two-profile retrieval we consider a joint retrieval of OH and O_3 . For multi-profile retrieval a smaller spectral window of 500 MHz, corresponding to the second autocorrelator segment of 4.5–5 GHz, is used. Based on the previous sensitivity analysis, the sensitivity of OH is highest in this spectral range. In Fig. 1 a pair of strong O_3 lines appears in the wings of the OH triplet, which implies that an uncertainty in the concentration profile of O_3 may have a distinct influence on the retrieval results of OH. To investigate how well OH can be retrieved without an accurate a priori knowledge of ozone, O_3 is retrieved simultaneously with OH.

For the joint retrieval of OH and O_3 we minimize (2) in conjunction with Eq. (5) for a set of regularization parameters $\boldsymbol{\lambda} = (\lambda_{OH}, \lambda_{O_3})$, and then compute the solution errors in each component, that is, $\epsilon_{OH}(\boldsymbol{\lambda}) = \|\mathbf{x}_{OH,\lambda} - \mathbf{x}_{OH,t}\|/\|\mathbf{x}_{OH,t}\|$ and $\epsilon_{O_3}(\boldsymbol{\lambda}) = \|\mathbf{x}_{O_3,\lambda} - \mathbf{x}_{O_3,t}\|/\|\mathbf{x}_{O_3,t}\|$, as well as the total solution error $\epsilon(\boldsymbol{\lambda}) = \sqrt{\epsilon_{OH}(\boldsymbol{\lambda})^2 + \epsilon_{O_3}(\boldsymbol{\lambda})^2}$. The results in Fig. 6 show that for $\lambda_{OH} = 1 \times 10^{-4}$ and λ_{O_3} ranging between 1×10^{-6} and 1, the total solution error is small and almost constant. However, in order to obtain smaller residual after convergence, the regularization parameters of OH and O_3 are set to $\lambda_{OH} = 1 \times 10^{-4}$ and $\lambda_{O_3} = 1 \times 10^{-6}$, respectively.

The relative differences of OH and O_3 are displayed in the left panel (a) of Fig. 7. Although O_3 is weakly regularized during the retrieval, an error of less than 5% is found below the observing altitude, however, an underestimate above 35 km can be observed. Concerning OH, errors of less than 15% with respect to the true profile in

266

both combinations are observed over the whole altitude range, that are comparable to the result of the one-profile fit. The right panel (b) of Fig. 7 illustrates the retrieval error, the smoothing and the noise errors for the retrieved molecules. The retrieval error is dominated by the smoothing error at lower altitudes and by the noise error above 25 km. It is apparent that the vertical resolution of the retrieval of OH is poorer than the O₃ retrieval. The smoothing error of O₃ is very small, which reveals that the main information comes from the measurement itself rather than from the a priori information.

3.2.3 Three-profile retrieval

Another aspect to consider is the three-profile retrieval. The state vector comprises three molecules, i.e. OH, O₃, and H₂O. The same spectral window as the two-profile retrieval is used. The regularization parameters $\lambda_{\text{OH}} = 1 \times 10^{-4}$, $\lambda_{\text{O}_3} = 2 \times 10^{-6}$, and $\lambda_{\text{H}_2\text{O}} = 5 \times 10^{-6}$ have been chosen by using the technique described in Sect. 3.2.2.

The difference with respect to the true profile in Fig. 8a shows that the OH retrieval can be done over the whole altitude range, although the errors are slightly larger than for the single- and two-profile retrievals. It may suggest that the inaccurate a priori knowledge of H₂O and O₃ could influence the OH retrieval. The retrieval error of OH in Fig. 8b is quite similar to the results above.

Using synthetic noisy measurements based on the perfect instrumental knowledge, the vertical concentration profile of OH can be retrieved in both single- and multi-profile retrieval frameworks in decent quality. A priori knowledge affects the retrieval error and yields a poor vertical resolution at lower altitudes, while the noise error dominates the retrieval error budget at higher altitudes. Although the spectral information over the instrument is limited, the profile of OH above 35 km can still be retrieved due to its high sensitivity in the middle stratosphere. Nonetheless, the imperfect instrumental knowledge and inaccurate atmospheric parameters can degrade the quality of retrieved solution.

267

3.3 Sensitivity to expected error sources

In the retrieval results displayed above, several assumptions of forward model profiles and instrument parameters have been made. However, it is of importance to see how imperfect atmospheric state profiles and instrumental knowledge influence the performance of the retrieval. For this reason, an error analysis has been carried out for atmospheric profiles and instrument parameters. In this study only the most important error sources (known from previous studies, e.g. de Lange et al., 2009, 2012; Baron et al., 2011; Urban et al., 2005) have been considered. As O₃ appears to be important in this OH microwindow, OH and O₃ were considered as the target molecules of multi-profile fitting involved in the following simulations. The selected regularization parameters are $\lambda_{\text{OH}} = 1 \times 10^{-4}$ and $\lambda_{\text{O}_3} = 1 \times 10^{-6}$. In contrast to Sect. 3.2, the initial and a priori profiles of the target molecules were scaled with a factor of 0.1, or rather, a priori error of 90%. H₂O, HCl, HOCl, and HO₂ were assumed to be known. In this study we concentrate on the performance of the OH retrieval affected by errors in calibration procedure, instrumental knowledge and atmospheric profiles.

3.3.1 Calibration error

Radiometric accuracy is crucial for a good quality of atmospheric profiles retrieval, especially systematic radiometric errors can result in a bias in the retrieval. For TELIS, a linear radiometric calibration approach is employed. An on-board blackbody unit is used as a hot signal reference and the signal from pointing into deep space is used as a cold signal reference. To reduce drift effects, both blackbodies are measured in short time intervals (ca. every 30 s) between the limb scans. From these hot and cold calibration measurements, the unknowns of the instrument's response function, the radiometric gain and the offset, can be determined and thus allow for a linear radiometric calibration of the measured spectra. However, in the TELIS IF-signal chain nonlinearities are present, which can not be compensated by the linear calibration approach and further lead to systematic errors in radiometric calibrated spectra. To study the

268

more severely influenced by larger biases (0.05 and 0.1). For more clarity, the large sideband ratio bias can result in significant error on the retrieval quality of OH.

In Fig. 12 the errors in terms of relative difference are obtained by retrievals with different η in the sideband ratio. The measurement is for the assumed sideband ratio $r = 1.0$. O_3 is not plotted for the reason that no significant error on the retrieved profile is induced by the sideband ratio bias. In our case, the intensity is sensitive to the contribution of OH in the upper sideband. As judged from Eq. (16) and Fig. 11, the retrieved OH profile is overestimated with positive biases on the sideband ratio, whereas underestimated with negative ones.

3.3.3 Instrumental knowledge: pointing

A pointing error can be characterized by systematic pointing bias and random pointing offset. The pointing error can be expressed by an altitude error at the tangent point, or by an error in the zenith angle of the line-of-sight. The MIPAS-B instrument on the gondola is equipped with a highly stable attitude and heading reference system (Friedl-Vallon et al., 2004). Although TELIS also receives its pointing information from this system, the stability of the connection between both instruments remains to be examined, a fact which could have an impact on the quality of the trace gas retrieval. It has been probed that the systematic pointing bias is 3.4 arcmin on the zenith angle for the 1.8 THz channel, corresponding to a 500 m deviation for the lowest tangent altitude (15 km) in this case.

Assuming that the uncertainty in this systematic pointing bias is up to 1 arcmin, the expected error propagation onto the retrieved profile of OH is plotted in Fig. 13. As this bias is deterministic, the propagated error is estimated by using Eq. (7) in the framework of a linearized forward model about the true state. A propagated error of up to 0.01 ppbv with the uncertainty of 1 arcmin is found below the observing altitude. As a result of very low concentration at lower altitude, the largest propagated error occurs between 15–25 km.

273

The relative differences in the OH profile for a single-target retrieval by assuming the uncertainties of 0.5 and 1 arcmin in the systematic pointing bias (3.4 arcmin) are shown in Fig. 14a. These results are in agreement with the relative propagated errors in Fig. 13b, leading to the conclusion that the forward model is not too nonlinear. The pointing error yields a shift of all gas profiles. As O_3 is the most important contributor to the measurement signal, an unresolved shift of the O_3 profile is the reason for the large relative differences in the OH profile. The relative differences in the OH profile become considerably smaller if a joint retrieval of OH and O_3 is performed, as can be seen in Fig. 14b.

The standard approach for far infrared and microwave limb sounding is to extract the pointing information from measurements of oxygen emission lines. Alternatively, the pointing error can be retrieved for each spectrum in the limb sequence together with the target molecules. In this case the random pointing offset is nearly compensated.

3.3.4 Atmospheric profiles

The accuracy of the temperature profile is vital to the reliability of target gas retrievals. For more precise retrieval results from actual TELIS data, the MIPAS-B temperature retrieval can be a pleasant candidate due to the fact that MIPAS-B and TELIS are both carried by the same gondola frame.

We have assumed an uncertainty of 1 K on the temperature profile for altitudes up to 45 km to investigate the corresponding effect on the retrieval. In Fig. 15, the estimated error propagation onto the retrieved OH profile via Eq. (7) is depicted. Below 27.5 km, the propagated error ranges 10–14 %. The profile is saturated and depleted by up to 0.0006 ppbv respectively with errors of 1 and -1 K in the temperature profile. Between 27.5 and 35 km, a propagated error of up to 7 % is found despite an increased absolute propagated error because of up to two orders of magnitude higher concentration in the stratosphere. It implies that a slight deviation in the temperature profile may cause an error especially at lower altitudes (upper troposphere and lower stratosphere) where the concentration of OH is relatively low.

274

a factor of 5, as compared to the results using the THz channel only. In this case, the relative retrieval error is therefore 5–10 % better over the altitude range of 10–20.5 km. For the retrieval using the THz channel only, the noise error dominates the retrieval error over the whole altitude range due to the worse signal-noise-ratio, whereas the noise error is very closed to zero for the retrieval with the GHz channel data. The smoothing error for all retrievals is large below 20.5 km and the regularization can have an effect on the retrieval quality of HCl. By comparison with the results using the GHz channel alone, a smaller smoothing error given by the multi-channel measurement is achieved, although a slightly worse retrieval error is found above 20.5 km due to larger measurement noise in the THz channel. According to these results, the sensitivity of HCl in the THz channel microwindow is superior to that in the GHz channel microwindow at higher altitudes, while at lower altitudes the GHz channel data delivers a stronger HCl signal.

In Fig. 17 the errors of HCl with respect to the true profile for the three cases are depicted. The error for the multi-channel measurement is overall better than that retrieved from the THz channel measurement. A large improvement can be found below 17.5 km with respect to that using the GHz channel only. The largest error appears around 20.5 km where the noise error (see Fig. 16b) is largest below the observer in the THz channel measurement.

These results indicate that the multi-channel simultaneous retrieval can help to improve the quality of the retrieval by significantly better exploitation of information from the observations. Furthermore, the multi-channel fitting requires less iteration steps than both single-channel cases.

5 Conclusions

We have presented the retrieval code PILS for infrared/microwave limb sounding and applied it to the TELIS level-2 data processing. Compared to most stochastic data models used in the literature, our data analysis operates in a semi-stochastic setting. The forward model is based on an optimized line-by-line code, coupled with automatic

differentiation for evaluating Jacobians accurately and efficiently, and the inversion employs nonlinear least squares fitting with direct and iterative multi-parameter regularization methods.

A sensitivity study of hydroxyl radical (OH) retrieval from spectra recorded by the TELIS 1.8 THz channel has been given, assuming a single limb scan with a worst case signal-noise-ratio, but otherwise perfect instrumental knowledge. Both single- and multi-profile retrieval frameworks perform in decent quality. The results illustrate that OH can be derived from the TELIS observations in the lower and middle stratosphere. The relative retrieval error is typically 25 % at the lowest altitude due to the a priori knowledge and gradually improves with increasing altitude where the retrieval error is dominated by the noise error.

Furthermore, a sensitivity analysis on potential error sources has been conducted. We have simulated the calibration procedure in the forward model and retrieved OH from the calibrated measurements distorted by nonlinearity. The calibration error, mainly the nonlinearity effect, does not introduce a severe error on the OH retrieval.

However, the inaccurate knowledge of the receiver sideband ratio is estimated to induce an error in the retrieval, because the strong OH line lies in the upper sideband in the selected frequency microwindow. The results are found to be more severely influenced by larger biases. In particular, the pointing error could be another major error source for the OH retrieval.

The propagated errors due to the atmospheric profiles have also been investigated. The OH retrieval is very sensitive to the errors in the temperature and pressure profiles at lower altitudes where the concentration is rather low.

Besides, the capability of multi-channel simultaneous retrieval of hydrogen chloride (HCl) from the far infrared and submillimeter observations has been studied. The errors and averaging kernels demonstrate the improvement on the retrieval quality, particularly over the lower altitude range.

There are some important issues to be resolved, such as pointing retrieval, reliable temperature profile, and errors in spectroscopic parameters and continuum model. Our

- Doicu, A., Trautmann, T., and Schreier, F.: Numerical Regularization for Atmospheric Inverse Problems, Springer and Praxis Publishing, Berlin Heidelberg, XIII, 1–426, doi:10.1007/978-3-642-05439-6, 2010. 258, 259
- Englert, C., Schimpf, B., Birk, M., Schreier, F., Krocka, M., Nitsche, R., Titz, R., and Summers, M.: The 2.5THz heterodyne spectrometer THOMAS: Measurement of OH in the middle atmosphere and comparison with photochemical model results, *J. Geophys. Res.*, 105, 22211–22223, doi:10.1029/2000JD900305, 2000. 255
- Fischer, H., Birk, M., Blom, C., Carli, B., Carlotti, M., von Clarmann, T., Delbouille, L., Dudhia, A., Ehhalt, D., Endemann, M., Flaud, J. M., Gessner, R., Kleinert, A., Koopman, R., Langen, J., López-Puertas, M., Mosner, P., Nett, H., Oelhaf, H., Perron, G., Remedios, J., Ridolfi, M., Stiller, G., and Zander, R.: MIPAS: an instrument for atmospheric and climate research, *Atm. Chem. Phys.*, 8, 2151–2188, doi:10.5194/acp-8-2151-2008, 2008. 275
- Fox, P., Hall, A., and Schryer, N.: The PORT Mathematical Subroutine Library, *ACM Trans. Math. Soft.*, 4, 104–126, doi:10.1145/355780.355789, 1978. 262
- Friedl-Vallon, F., Maucher, G., Seefeldner, M., Trieschmann, O., Kleinert, A., Lengel, A., Keim, C., Oelhaf, H., and Fischer, H.: Design and characterization of the balloon-borne Michelson Interferometer for Passive Atmospheric Sounding (MIPAS-B2), *Appl. Opt.*, 43, 3335–3355, doi:10.1364/AO.43.003335, 2004. 253, 273
- Griewank, A.: *Evaluating Derivatives: Principles and Techniques of Algorithmic Differentiation*, SIAM, Philadelphia, PA, 2000. 261
- Hascoët, L. and Pascual, V.: The Tapenade automatic differentiation tool: Principles, model, and specification, *ACM Trans. Math. Soft.*, 39, 3, doi:10.1145/2450153.2450158, 2013. 261
- Hedelt, P., Alonso, R., Brown, T., Collados Vera, M., Rauer, H., Schleicher, H., Schmidt, W., Schreier, F., and Titz, R.: Venus transit 2004: Illustrating the capability of exoplanet transmission spectroscopy, *A & A*, 533, A136, doi:10.1051/0004-6361/201016237, 2011. 261
- Jucks, K., Johnson, D., Chance, K., Traub, W., Margitan, J., Osterman, G., Salawitch, R., and Sasano, Y.: Observations of OH, HO₂, H₂O, and O₃ in the upper stratosphere: Implications for HO_x photochemistry, *Geophys. Res. Lett.*, 25, 3935–3938, doi:10.1029/1998GL900009, 1998. 254
- Kasai, Y., Sagawa, H., Kreyling, D., Suzuki, K., Dupuy, E., Sato, T. O., Mendrok, J., Baron, P., Nishibori, T., Mizobuchi, S., Kikuchi, K., Manabe, T., Ozeki, H., Sugita, T., Fujiwara, M., Irimajiri, Y., Walker, K. A., Bernath, P. F., Boone, C., Stiller, G., von Clarmann, T., Orphal, J., Urban, J., Murtagh, D., Llewellyn, E. J., Degenstein, D., Bourassa, A. E., Lloyd, N. D., Froidevaux,

- L., Birk, M., Wagner, G., Schreier, F., Xu, J., Vogt, P., Trautmann, T., and Yasui, M.: Validation of stratospheric and mesospheric ozone observed by SMILES from International Space Station, *Atmos. Meas. Tech. Discuss.*, 6, 2643–2720, doi:10.5194/amtd-6-2643-2013, 2013. 279
- Kikuchi, K., Nishibori, T., Ochiai, S., Ozeki, H., Irimajiri, Y., Kasai, Y., Koike, M., Manabe, T., Mizukoshi, K., Murayama, Y., Nagahama, T., Sano, T., Sato, R., Seta, M., Takahashi, C., Takayanagi, M., Masuko, H., Inatani, J., Suzuki, M., and Shiotani, M.: Overview and early results of the Superconducting Submillimeter-Wave Limb-Emission Sounder (SMILES), *J. Geophys. Res.*, 115, D23306, doi:10.1029/2010JD014379, 2010. 253
- Landgraf, J. and Hasekamp, O. P.: Retrieval of tropospheric ozone: The synergistic use of thermal infrared emission and ultraviolet reflectivity measurements from space, *J. Geophys. Res.*, 112, D08310, doi:10.1029/2006JD008097, 2007. 275
- Liou, K.-N.: *An Introduction to Atmospheric Radiation*, Academic Press, 2nd Edn., 2002. 256
- Mair, U., Krocka, M., Wagner, G., Birk, M., Hübers, H.-W., Richter, H., Semenov, A., Hoogeveen, R., de Graauw, T., Yagoubov, P., Maurellis, A., Selig, A., Koshelets, V., Shitov, S., Goltsman, G., Voronov, B., Ellison, B., Kerridge, B., Matheson, D., Siddans, R., and Reburn, J.: TELIS – Development of a New Balloon Borne THz/Submm Heterodyne Limb Sounder, in: *Proceedings of the 14. International Symposium on Space Terahertz Technology*, Tucson, AZ, USA, April 2003, 204–214, 2004. 255
- Melsheimer, C., Verdes, C., Bühler, S., Emde, C., Eriksson, P., Feist, D., Ichizawa, S., John, V., Kasai, Y., Kopp, G., Koulev, N., Kuhn, T., Lemke, O., Ochiai, S., Schreier, F., Sreerekha, T., Suzuki, M., Takahashi, C., Tsujimaru, S., and Urban, J.: Intercomparison of general purpose clear sky atmospheric radiative transfer models for the millimeter/submillimeter spectral range, *Radio Sci.*, 40, RS1007, doi:10.1029/2004RS003110, 2005. 261
- Mendrok, J., Schreier, F., and Höpfner, M.: Estimating cirrus cloud properties from MIPAS data, *Geophys. Res. Lett.*, 34, L08807, doi:10.1029/2006GL028246, 2007. 261
- Minschwaner, K., Manney, G. L., Wang, S. H., and Harwood, R. S.: Hydroxyl in the stratosphere and mesosphere – Part 1: Diurnal variability, *Atmos. Chem. Phys.*, 11, 955–962, doi:10.5194/acp-11-955-2011, 2011. 255
- Murtagh, D., Frisk, U., Merino, F., Ridal, M., Jonsson, A., Stegman, J., Witt, G., Eriksson, P., Jiménez, C., Megie, G., de la Noë, J., Ricaud, P., Baron, P., Pardo, J. R., Hauchcorne, A., Llewellyn, E. J., Degenstein, D. A., Gattinger, R. L., Lloyd, N. D., Evans, W. F., McDade, I. C., Haley, C. S., Sioris, C., von Savigny, C., Solheim, B. H., McConnell, J. C., Strong,

Table 1. Major instrument and geometry parameters used for simulating the synthetic spectra observed for the OH microwindow. The channel notation THz stands for the 1.8 THz channel.

Parameter	Description
Channel	THz
LO frequency	1830.10 GHz
Intermediate frequency	4–6 GHz
Spectral resolution	2.16 MHz
ILS function	Hamming apodization
Field-of-view (FWHM)	Gaussian (6.3 arcmin)
Sideband ratio	1.0
Signal-to-noise ratio	35
Top-of-atmosphere	85 km
Observing altitude	35 km
Tangent altitudes	15–33 km
Vertical sampling	2 km

Table 2. Major instrument and geometry settings for multi-channel retrieval simulation. The channel notation GHz stands for the 480–650 GHz channel.

Parameter	Description	
Channel	THz	GHz
LO frequency	1877.63 GHz	619.10 GHz
Intermediate frequency	4–6 GHz	5–7 GHz
ILS function	Hamming apodization	Lorentzian
Field-of-view (FWHM)	Gaussian (6.3 arcmin)	Gaussian (10.8 arcmin)
Signal-to-noise ratio	30	110
Top-of-atmosphere		85 km
Observing altitude		34 km
Tangent altitudes		10–32.5 km
Vertical sampling		1.5 km

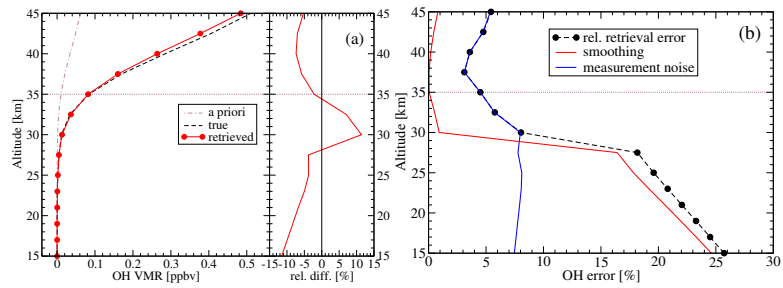


Fig. 5. Results of single OH retrieval and corresponding diagnostic quantities as a function of altitude. **(a):** retrieved VMR profile and corresponding errors in terms of relative difference with respect to the true profile. The dashed black line refers to the true profile. **(b):** corresponding properties of the retrieval, i.e. relative retrieval error, smoothing and noise errors.

291

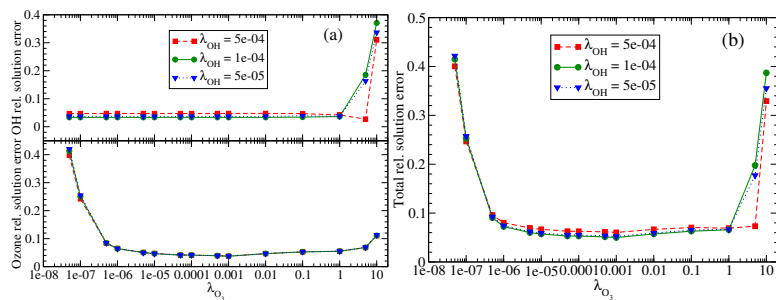


Fig. 6. Determination of the regularization parameters for two-profile retrieval of OH and O_3 . **(a):** relative solution errors of OH and O_3 versus different regularization parameters of OH and O_3 . **(b):** total solution errors versus the regularization parameters of OH and O_3 .

292

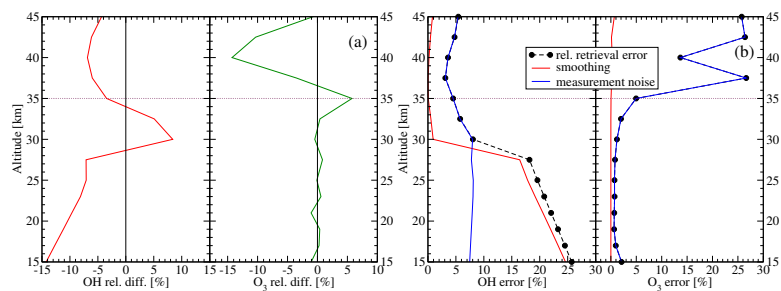


Fig. 7. Retrieval results for two-profile retrieval as a function of altitude. **(a):** relative differences for joint retrieval of OH and O₃. **(b):** relative retrieval error, smoothing and noise errors for joint retrieval of OH and O₃.

293

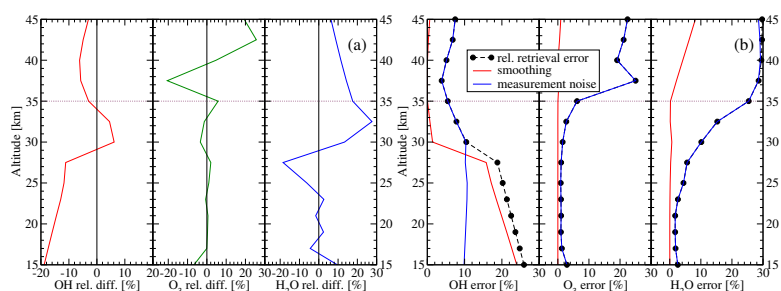


Fig. 8. Retrieval results for three-profile retrieval as a function of altitude. **(a):** relative differences for joint retrieval of OH, O₃, and H₂O. **(b):** relative retrieval error, smoothing and noise errors for joint retrieval of OH, O₃, and H₂O.

294

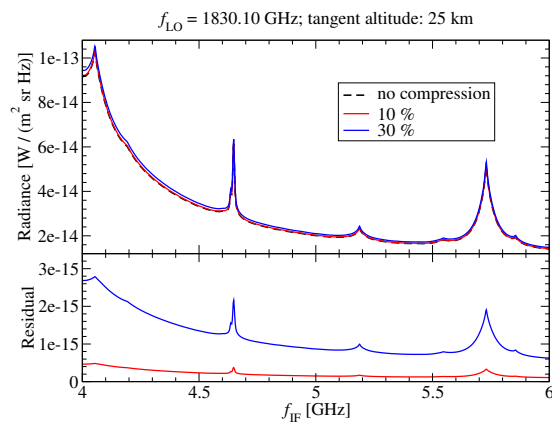


Fig. 9. Modelled calibrated spectrum measured at the tangent altitude of 25 km and corresponding residuals with respect to the pure model spectrum. The assumed compressions of 10 and 30 % in the hot load measurement are taken into account.

295

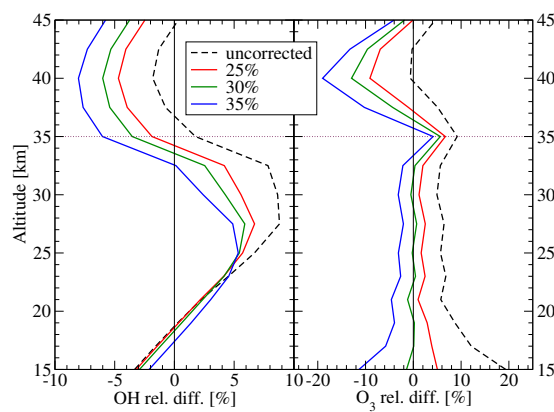


Fig. 10. Relative difference of OH and O₃. The retrievals are done for the noisy synthetic measurements that are generated by the calibrated spectra with the compression of 30 % in the hot load. 5 % uncertainty is taken into account in the pseudo-correction procedure: the compression is set to 25 and 35 % for two repeated retrievals.

296

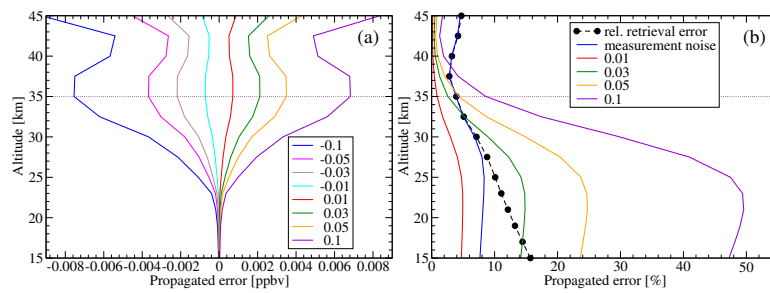


Fig. 11. Propagated error of sideband ratio onto the OH retrieval with the sideband ratio bias η . **(a)**: results in terms of absolute unit (VMR) with respect to the values ± 0.01 , ± 0.03 , ± 0.05 , and ± 0.1 for η . **(b)**: results in terms of relative unit in percent of the true profile with respect to the positive values for η . For reference the retrieval error and the noise error caused by the measurement noise are included in this plot.

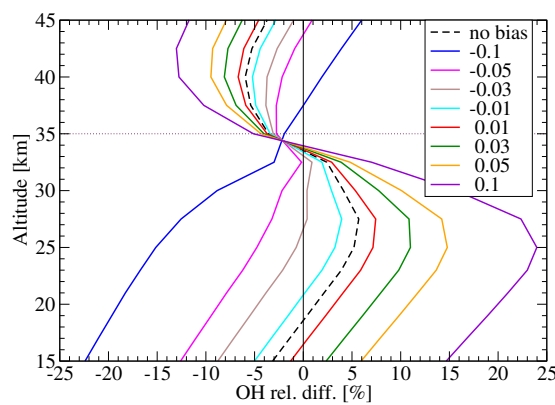


Fig. 12. Errors for OH retrieval in terms of relative difference with different values of relative bias η in the sideband ratio. The retrievals are performed using the synthetic measurement for ideal sideband ratio $r = 1.0$. For reference the retrieval result for the assumed sideband ratio $r = 1.0$ is given in dashed black line.

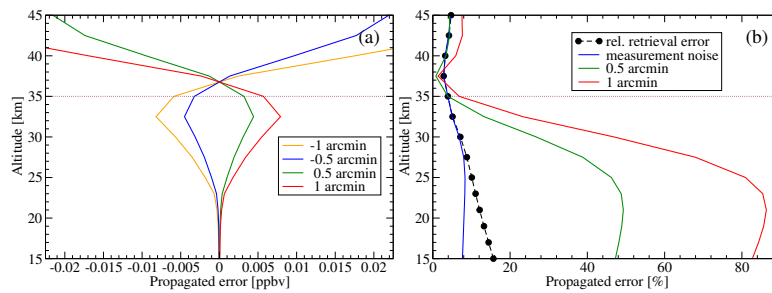


Fig. 13. Propagated error of pointing onto the OH retrieval with the error on the systematic pointing bias. By assuming ± 0.5 and ± 1 arcmin, respectively, the results in terms of absolute unit **(a)** and relative unit **(b)** with respect to the true profile are shown.

299

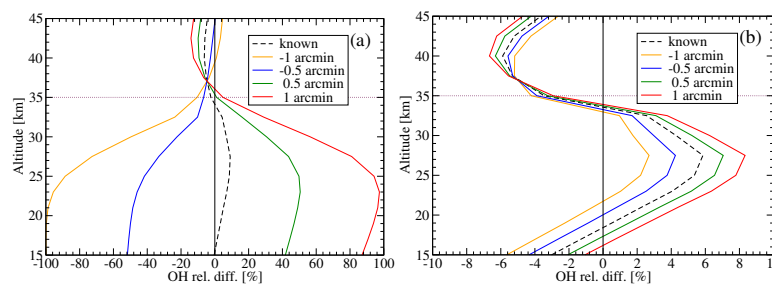


Fig. 14. Relative differences in the OH profile for single-target retrieval **(a)** and joint retrieval of OH and O₃ **(b)** with uncertainties of 0.5 and 1 arcmin in the systematic pointing bias. For reference the retrieval result for the perfectly known pointing information is given in dashed black line.

300

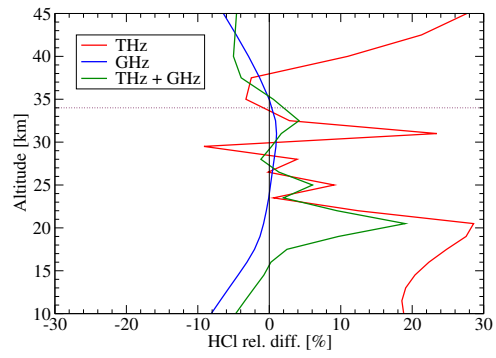


Fig. 17. Relative differences of HCl for the single- and multi-channel retrievals. The retrievals are done with the THz, GHz, and the combination of THz and GHz data, respectively.